Nuclear relaxation of ^{3}He in the presence of O_2

B. Saam, W. Happer, and H. Middleton
Department of Physics, Princeton University, Princeton, New Jersey 08544
(Received 6 December 1994)

We have measured the longitudinal nuclear relaxation rate T_1^{-1} for ^{3}He in the presence of molecular oxygen in the temperature range $T \approx 200$–400 K. At room temperature, $T_1^{-1} = 0.448 \pm 0.010$ s^{-1} per amagat O_2, in approximate agreement with theoretical models for intermolecular dipolar relaxation. Furthermore, in this temperature range, $T_1^{-1} \propto T^{-0.42\pm0.04}$. Our results are of practical importance for the growing number of applications involving hyperpolarized noble gases.

PACS number(s): 34.20.Gj, 33.25.+k

Recent developments in the application of nuclear spin-polarized noble gases, particularly to magnetic resonance imaging (MRI) [1,2], have focused attention on the nuclear relaxation of these gases in a variety of environments. These applications often depend on enhancement of the polarization by several orders of magnitude over thermal equilibrium, e.g., through spin exchange with an optically pumped alkali-metal vapor [3–5]. Since it is in a highly nonequilibrium state, the utility of such a hyperpolarized sample is critically dependent on its longitudinal relaxation time T_1, which is most often dominated by interactions with the container surface, or by interactions with other gas-phase impurities.

For noble-gas MRI, particularly in biological environments, paramagnetic molecular oxygen is a very potent and perhaps the most important source of relaxation. Measurements of oxygen's effect on T_1 for ^{129}Xe have already been carried out [6]. We present measurements of T_1 for ^{3}He in the presence of up to 8 amagats of O_2 for temperatures in the range 200–400 K. (The amagat is a unit of density equal to the number of molecules per unit volume of an ideal gas at 0° C and normal atmospheric pressure.)

The study of nuclear relaxation of noble gases in the presence of oxygen is greatly simplified by the lack of significant competing mechanisms for even modest (> 0.1 amagat) values of $[O_2]$. Long T_1's (many hours) are possible in pure noble-gas samples because the electrons in the filled orbitals of an isolated noble-gas atom produce neither an electric-field gradient nor a magnetic field at their nucleus. Since noble gases are monatomic, there are also no intramolecular interactions with other nearby magnetic moments. Surface residence times, particularly for ^{3}He, are short enough that T_1 is at least tens of minutes in a reasonably clean, sealed glass cell. However, for an impurity concentration as small as $[O_2] = 0.1$ amagat, intermolecular dipolar relaxation reduces T_1 to about 20 s for ^{3}He.

If all ^{3}He relaxation occurs during isolated binary collisions with O_2 molecules, then $T_1^{-1} = T_2^{-1}$, and T_1^{-1} depends linearly on $[O_2]$ at a given temperature and magnetic field. Isolated binary collisions prevail when $\tau_c \ll \tau_b$, where τ_c and τ_b are the duration of and the time between collisions, respectively. Using typical values for the gas-kinetic cross section and the characteristic intermolecular interaction length, it is straightforward to show that this condition holds for total gas densities up to at least several tens of amagats.

For our experiment, a set of five sealed cells (≈ 1 cm^3) made of Corning 7740 (Pyrex^{TM}) glass were prepared on a high-purity gas-handling system using techniques similar to those detailed in [7,8]. The contents of each cell are summarized in Table I. The cells were filled successively through a single glass manifold attached to the gas-handling system. Before filling, each cell was first cooled to ≤ 20 K by a small flowing-liquid-helium Dewar. The appropriate quantity of oxygen, admitted from a calibrated volume at a known temperature and pressure, was then allowed to condense into the cold cell. Finally, about 5 amagats of ^{3}He were introduced, before the cell was flame sealed from the manifold. The cell volumes were later determined to $\leq 0.5\%$ by buoyant-weight measurements and the application of Archimedes's principle.

Measurements of the longitudinal relaxation time T_1 of ^{3}He were made for each cell at each of three different temperatures in an applied magnetic field $B_0 = 14.1$ kG. To obtain data at 197 K, the probe was immersed in a cryogenic bath of CCl_3F containing dry ice. At 369 K, the probe was placed in an aluminum oven heated by flowing air. Data were also taken at room temperature. The results are shown in Fig. 1 and Table II. In Fig. 2 we plot the per-amagat relaxation rate (the "All cells" column in Table II) vs temperature on a log-log scale. We thus obtain an empirical formula for longitudinal relaxation of ^{3}He in the presence of O_2 for $T \approx 200$–400 K:

$$\frac{1}{T_1} = 0.45[O_2]\left(\frac{299}{T}\right)^{0.42} \text{ s}^{-1}/\text{amagat}, \qquad (1)$$

TABLE I. Summary of contents for the five cells.

Cell no.	Volume cm^3	[^{3}He] (amagat)	[O_2] (amagat)
1	0.8995 ± 0.003	5.31 ± 0.05	0.969 ± 0.004
2	0.884 ± 0.003	5.23 ± 0.05	7.92 ± 0.02
3	0.881 ± 0.003	5.25 ± 0.05	3.97 ± 0.01
4	0.9435 ± 0.003	4.84 ± 0.05	1.856 ± 0.006
5	0.840 ± 0.003	4.90 ± 0.05	0

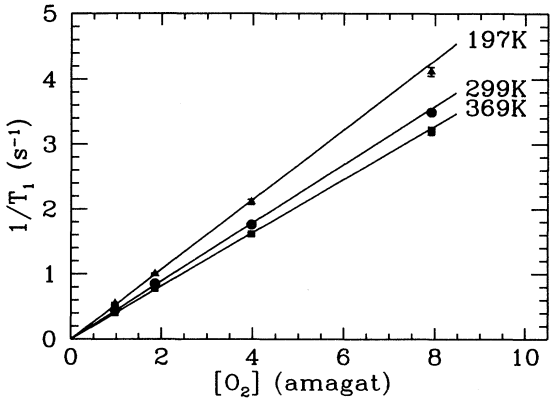

FIG. 1. Relaxation rate T_1^{-1} of ^{3}He plotted vs $[O_2]$. The lines are linear fits through the origin at each temperature and correspond to the "All cells" column in Table II.

TABLE II. T_1^{-1} of ^{3}He per amagat of O_2. The "All cells" column is based on a weighted average of data from all four cells. The "Densest cell" column is based only on the cell for which $[O_2] \approx 8$ amagats.

T	$(T_1[O_2])^{-1}$ (s^{-1}/amagat)	
(Kelvin)	All cells	Densest cell
197 ± 1	0.537 ± 0.020	0.520 ± 0.009
299 ± 1	0.448 ± 0.010	0.441 ± 0.004
369 ± 2	0.410 ± 0.010	0.405 ± 0.007

where $[O_2]$ is in amagats, the leading coefficient is the measured per-amagat relaxation rate at 299 K (see Table II), and the exponent is the fitted slope in Fig. 2.

A single-coil quadrature-detection pulse-NMR spectrometer, operating near the ^{3}He Larmor frequency $\omega_L = 2\pi \times 45.67$ MHz, was used to deliver a saturation-recovery ($\pi/2$-t-$\pi/2$) rf-pulse sequence [9] and to receive the signal from the subsequent free-induction decay (FID). A digital oscilloscope recorded and averaged up to 36 FID's for a given recovery time t. The averaged signals, acquired over an appropriate range for t, were downloaded and analyzed using the LabWindows^{TM} utility from National Instruments.

A fast Fourier transform was performed on each averaged FID with the resulting spectrum windowed about the absorption line and integrated to give the total signal strength $S(t)$. Choice of an appropriately large frequency window and integration of the line shape negated short-term drifts in B_0 which occurred while averaging. Long-term drifts were adequately reduced using a separate NMR stabilizer locked to the ^{19}F resonance. Figures 3(a) and 3(b) show a typical averaged absorption spectrum along with that from a single acquisition for comparison. Figure 3(c) shows a typical plot of $S(t)$ vs t. A least-squares fit to

$$S(t) = S_0 \left[1 - \exp\left(\frac{-(t+t_0)}{T_1}\right)\right], \qquad (2)$$

where S_0 and t_0 are free parameters, is used to extract T_1. The saturated thermal-equilibrium signal is S_0, and t_0 determines the average residual signal at $t = 0$ resulting from any small error in the first $\pi/2$ pulse or from rf-field inhomogeneities across the sample.

Results of T_1 measurements on a fifth cell, nominally having $[O_2] = 0$, constrain all three lines in Fig. 1 to pass through the origin. During production, this cell was sealed from the manifold last and thus presumably subject to the greatest contamination from residual O_2 or other impurities. Yet we measured $T_1 \geq 20$ min at $T = 197$ K (even longer at higher temperatures) for this cell, from which we conclude that the residual relaxation rate due to wall collisions and other impurities in the

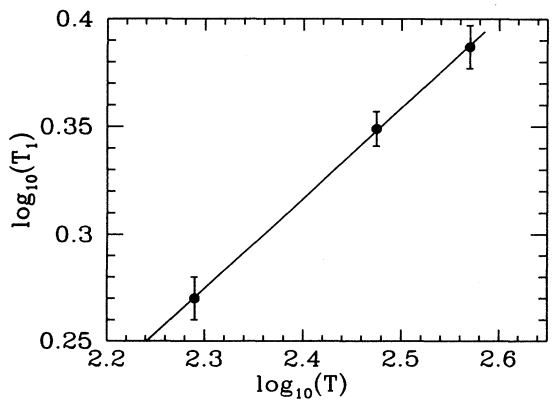

FIG. 2. The slope of each line in Fig. 1 vs the corresponding absolute temperature on a log-log plot. The slope implies $T_1^{-1} \propto T^{-0.42 \pm 0.04}$ in this temperature range.

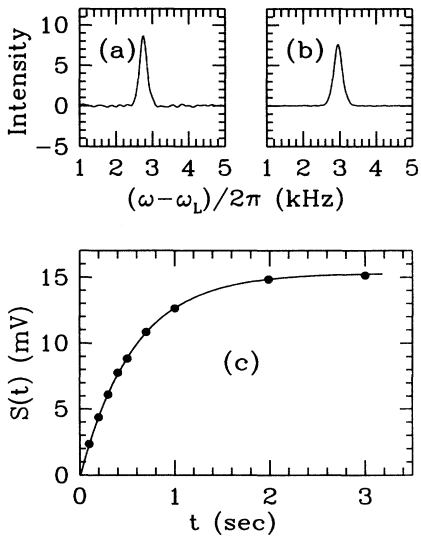

FIG. 3. Typical spectrum of a single acquisition (a) and an average of 16 acquisitions (b). The line shape is determined by the inhomogeneity in B_0. The averaged line is slightly smaller and broader due to drifts in B_0 during averaging. A fit to Eq. (2) of room-temperature data for the cell with $[O_2] \approx 4$ amagats is shown in (c). Each of the points in (c) is the result of integrating an absorption peak like the one in (b).

other four cells is negligible.

For each temperature, the per-amagat relaxation rate is calculated by considering the slopes of four separate lines connecting the origin and each of the four data points. The analysis is done this way to incorporate the error in $[O_2]$ for each cell. A systematic trend in the slopes is observed. The total decrease in slope from lowest to highest $[O_2]$ is about 5% at 299 K, while measurement error for each point is about 1%. A similar monotonic decrease is observed in the data taken at the other two temperatures. We propose below a possible explanation for this trend based on diffusion of spins from the stem of the cell between the two rf pulses. If this explanation is correct, then the best T_1 measurements come from the cells with the highest $[O_2]$ (lowest diffusion constant). With this in mind, Table II gives two values of the per-amagat relaxation rate for each temperature. The first value, on which our data analysis is based, is a weighted average of all four slopes with the error increased to accommmodate the systematic trend. The second value is based solely on T_1 for the cell with $[O_2] \approx 8$ amagats. If in fact the second value is more accurate, the leading coefficient in (1) should be changed to 0.44 and the temperature exponent to 0.40.

As pointed out by Jameson, Jameson, and Hwang [6], both kinetic-theory [10] and correlation-function [11] approaches to gas-phase intermolecular dipolar relaxation lead to the following expression for T_1^{-1} for ^{3}He in the presence of O_2:

$$\frac{1}{T_1} = \frac{16}{3} S(S+1)\gamma_I^2\gamma_S^2 \frac{\hbar^2}{d^2}\left(\frac{\pi\mu}{8k_BT}\right)^{1/2}[O_2]F(V,T), \quad (3)$$

where $S = 1$ is the O_2 spin, γ_I and γ_S are the gyromagnetic ratios for ^{3}He and O_2, respectively, d is the characteristic intermolecular interaction length, μ is the ^{3}He-O_2 reduced mass, k_B is the Boltzmann constant, and T is the absolute temperature. The factor in parentheses is the reciprocal mean relative velocity $\bar{v}^{-1}$. The function $F(V,T)$ carries information specific to the ^{3}He-O_2 interatomic potential V and approaches unity in the hard-sphere high-temperature limit. The expression (3) is for the zero-field limit $(\omega_S\tau_c)^2 \ll 1$, where $\omega_S = \gamma_s B_0$. This limit is easily satisfied at an applied magnetic field $B_0 = 14$ kG, and corresponds to an O_2 spin not having enough time to precess significantly around $\mathbf{B}_0$ during a collision. We note that a term proportional to $|\psi(0)|^4$ should in general be included in $F(V,T)$ corresponding to a Fermi-contact hyperfine term, where $\psi(0)$ is the amplitude for finding an O_2 electron at the ^{3}He nucleus.

We can estimate T_1^{-1} from (3), assuming the hard-sphere high-temperature limit where $F(V,T) \to 1$. We choose $d = 3.1$ Å, which corresponds to the classical turning point for the isotropic portion of the He-O_2 interatomic potential [12]. Equation (1) deviates from the $T^{-1/2}$ dependence in (3), which is expected at finite temperatures, and the anisotropic pieces of the interatomic potential [13,14] as well as any Fermi-contact interaction have been neglected. Nevertheless, (3) predicts $T_1^{-1} = 0.28\ \mathrm{s}^{-1}$/amagat at 299 K, less than a factor of 2 smaller than our measured value.

A rigorous theoretical calculation of $F(V,T)$ involves integrating solutions of the radial Schrödinger equation for the intermolecular potential over the Boltzmann distribution of relative collisional momenta. For the weakly interacting ^{3}He-O_2 system at room temperature, $\epsilon/k_BT \sim 0.01$ [12], where ϵ characterizes the depth of the intermolecular potential well. The well depth is a factor of 5 larger for Ar-O_2 [12] and should be still larger for Xe-O_2. Relaxation of ^{3}He may thus be much less sensitive to the details of the intermolecular potential than that of ^{129}Xe. This is further suggested by the relatively close agreement of our ^{3}He-O_2 data with the hard-sphere limit of (3). At room temperature, we conclude from our data that $F(V,T) = 1.7$, whereas $F(V,T) \approx 6$ for ^{129}Xe-O_2 [6].

Finally, we believe that the small deviation from linearity in our data can be explained by gaseous diffusion. The cells each have a small stem, comprising about 15% of the cell volume, which is outside the solenoidal probe coil. Both rf-field intensity and detection efficiency are thus reduced in the stem. A smaller rf field means that the initial pulse does not fully destroy the polarization in this region. In the limit of no diffusion, this residual polarization does not affect the T_1 measurement, since the polarization everywhere recovers with the same T_1. This limit is defined by $\sqrt{DT_1} \ll L$, where L is a characteristic length of the sample and D is the diffusion constant of the ^{3}He. However, if diffusion is fast ($\sqrt{DT_1} \gtrsim L$), the residual polarization in the stem diffuses into the main body of the cell between the two rf pulses and is then detected more efficiently. The result is a shorter apparent T_1, which arises from a combination of O_2-induced nuclear relaxation and diffusion-mode relaxation rates. For the cell with $[O_2] \approx 8$ amagats, $\sqrt{DT_1} \approx 0.1$ cm, while for the cell with $[O_2] \approx 1$ amagat, $\sqrt{DT_1} \approx 0.8$ cm. Given $L \approx 1$ cm, those cells with lower $[O_2]$ are in the regime where diffusion could alter the measured value of T_1. This effect is necessarily small, since the stem comprises only a small portion of the total volume, and the initial pulse does destroy some polarization there. Calculations based on a simplified cell shape and estimates of the rf field in the stem indicate that it is reasonable to expect the observed few-percent effect.

ACKNOWLEDGMENTS

We thank B. Driehuys and M. S. Conradi for helpful discussions, the latter in particular for sharing his excellent design for a pulse-NMR spectrometer. This work was supported by the NSF Engineering Research Council and by AFOSR Grant No. F49620-92-J-0211.

[1] M.S. Albert, G.D. Cates, B. Driehuys, W. Happer, B. Saam, C.S. Springer, Jr., and A. Wishnia, Nature (London) **370**, 199 (1994).
[2] H. Middleton, R.D. Black, B. Saam, G.D. Cates, G.P. Cofer, B. Guenther, W. Happer, L.W. Hedlund, G.A. Johnson, K. Juvan, and J. Swartz, Magn. Res. Med. **33**, 271 (1995).
[3] N.D. Bhaskar, W. Happer, and T. McClelland, Phys. Rev. Lett. **49**, 25 (1982).
[4] W. Happer, E. Miron, S. Schaefer, D. Schreiber, W.A. van Wijngaarden, and X. Zeng, Phys. Rev. A **29**, 3092 (1984).
[5] G.D. Cates, R.J. Fitzgerald, A.S. Barton, P. Bogorad, M. Gatzke, N.R. Newbury, and B. Saam, Phys. Rev. A **45**, 4631 (1992).
[6] C.J. Jameson, A.K. Jameson, and J.K. Hwang, J. Chem. Phys. **89**, 4074 (1988).
[7] N.R. Newbury, A.S. Barton, G.D. Cates, W. Happer, and H. Middleton, Phys. Rev. A **48**, 4411 (1993).
[8] H. Middleton, Ph.D. thesis, Princeton University, 1994 (unpublished).
[9] E. Fukushima and S.B.W. Roeder, *Experimental Pulse NMR: A Nuts and Bolts Approach* (Addison-Wesley, Reading, MA, 1981).
[10] F.M. Chen and R.F. Snider, J. Chem. Phys. **46**, 3937 (1967).
[11] I. Oppenheim and M. Bloom, Can. J. Phys. **39**, 845 (1961).
[12] F. Battaglia, F.A. Gianturco, P. Casavecchia, F. Pirani, and F. Vecchiocattivi, Faraday Discuss. Chem. Soc. **73**, 257 (1982).
[13] M. Faubel, K.H. Kohl, J.P. Toennies, and F.A. Gianturco, J. Chem. Phys. **78**, 5629 (1983).
[14] J.H. van Lenthe and F.B. van Duijneveldt, J. Chem. Phys. **81**, 3168 (1984).